The Journal of Chemical Physics

Engineering adjustable two-pore devices for parallel ion transport and DNA translocations

Cite as: J. Chem. Phys. **154**, 105102 (2021); https://doi.org/10.1063/5.0044227
Submitted: 14 January 2021 . Accepted: 19 February 2021 . Published Online: 10 March 2021

Yung-Chien Chou, Joshua Chen, Chih-Yuan Lin, and Marija Drndić

The Journal of hemical Physics ARTICLE scitation org/journal/jcp

Engineering adjustable two-pore devices for parallel ion transport and DN translocations

Cite as: J. Chem. Phys. 154, 105102 (2021); doi: 10.1063/5.0044227
Submitted: 14 January 2021 ccepted: 19 February 2021
Published Online: 10 March 2021

Yung-Chien Chou, Joshua Chen, Chih-Yuan Lin, and Marija Drndić[a)]

FFILI TIONS

Department of Physics and stronomy, University of Pennsylvania, Philadelphia, Pennsylvania 19104, US

Note: This paper is part of the J P Special Topic on Fluids in Nanopores.
[a)] **uthor to whom correspondence should be addressed:** drndic@physics.upenn.edu

BSTR CT

We report ionic current and double-stranded DNA (dsDNA) translocation measurements through solid-state membranes with two TEM-drilled ~3-nm diameter silicon nitride nanopores in parallel. Nanopores are fabricated with similar diameters but varying in effective thicknesses (from 2.6 to 10 nm) ranging from a thickness ratio of 1:1 to 1:3.75, producing distinct conductance levels. This was made possible by locally thinning the silicon nitride membrane to shape the desired topography with nanoscale precision using electron beam lithography (EBL). Two nanopores are engineered and subsequently drilled in either the EBL-thinned or the surrounding membrane region. By designing the interpore separation a few orders of magnitude larger than the pore diameter (e.g., ~900 vs 3 nm), we show analytically, numerically, and experimentally that the total conductance of the two pores is the sum of the individual pore conductances. For a two-pore device with similar diameters yet thicknesses in the ratio of 1:3, a ratio of ~1:2.2 in open-pore conductances and translocation current signals is expected, as if they were measured independently. Introducing dsDNA as analytes to both pores simultaneously, we detect more than 12 000 events within 2 min and trace them back with a high likelihood to which pore the dsDNA translocated through. Moreover, we monitor translocations through one active pore only when the other pore is clogged. This work demonstrates how two-pore devices can fundamentally open up a parallel translocation reading system for solid-state nanopores. This approach could be creatively generalized to more pores with desired parameters given a sufficient signal-to-noise ratio.

INTRODUCTION

Solid-state nanopore sensors are promising systems for single molecule detection and analysis.[1–7] Most studies have focused on single-pore devices, and only a few have considered implementing multiple pores and the related possibilities. Recently, silicon nitride (SiN) and nanocapillary device geometries were demonstrated for DNA preconfinement[8] and entropic trapping[9] using a nanoporous membrane on top of a single sensing SiN pore. Additionally, several two-pore device geometries were demonstrated to control DNA transport by threading the DNA ends through the pores to achieve a "tug-of-war" scenario where the DNA ends may be pulled in opposite directions on two sides, and the DNA "flossed" back and forth, assuming sufficient control can be achieved.[10–17] An ionic signal from three pores in parallel, drilled in the same SiN membrane, has also been reported in multiplexed FET nanowire-nanopore devices. The signals from FETs near the pores acted as time-trackers when the DNA passed through that pore, showing the additive nature of DNA signals from individual pores to produce the measured two-terminal signal.[18]

The total conductance, G, of linear [$G \sim N \log(N)$] and square ($G \sim \sqrt{N}$) arrays of N pores was shown to depend on the geometry of the array and to scale sub-linearly with the number of pores, N, when the pore diameter, d, is similar to the interpore distance, L.[19] This was previously demonstrated experimentally with large SiN nanopores of diameters $d \sim 200$ nm made by focused ion beam milling and interpore separation $L \sim d$. For linear arrays with L larger than ~10d, G is the sum of individual pore conductances. Otherwise, for tightly packed arrays, G is smaller than the sum of individual pore conductances, which occurs as a consequence of the

overlapping electric field lines between nearby pores, shown to result in increased access resistance.[19]

Here, we fabricate and measure nanopore devices with two SiN nanopores of much smaller diameters d than in the previous studies[19] where, in addition to the diameter, the individual nanopore thickness is also a variable parameter. The pore diameters are just slightly larger than the width of double-stranded DNA (d_{DNA} = 2.2 nm) such that the DNA blocks a large fraction of the pore. Thus, the resulting DNA translocation signals are comparable to the open pore current signal and, combined with optimized chips,[20] produce a high signal-to-noise ratio (SNR) at bandwidths up to 1 MHz in this study. In our devices, the interpore separation L is fabricated to be >100 nm, two orders of magnitude larger than the pore diameters, $d \sim 3$ nm.

F BRIC TION OF TWO-PORE DEVICES

A schematic of advanced two-pore devices fabricated onto a suspended SiN window is demonstrated in Fig. 1(a). Prior to nanopore fabrication via TEM, the 5-mm-large chips, composed of, from bottom to top, a 500-μm silicon substrate, a 5-μm thermal SiO_2, and a 30-nm low-stress SiN, are made through traditional microfabrication methods[21,22] to create a suspended SiN membrane window. We then use electron beam lithography to pattern a set of four squares, 200 by 200 nm^2, onto the SiN membrane. Combining this with reactive ion etching (RIE) with trifluoromethane and oxygen (CHF_3/O_2) at a rate of ~1 nm/s, similar to previous procedures,[21,22] we are able to remove SiN within the patterned area to the desired thickness. High-resolution TEM mode, operating at 200 kV with an electron beam current of 20 nA, is then used to locate the region of interest and to fabricate nanopores.[20]

We here demonstrate two model versions of such two-pore devices with pore diameters from 3 to 4 nm and pore separations from 900 nm to 2 μm. The membrane thicknesses (t = 30 and 8 nm) are controlled with a precision of ±1 nm by RIE to remove SiN[21,22] and adjusted so that the two pores have the same or different sensitivities to the analyte. Specifically, the pores have similar diameters ($d_1 \sim d_2$) but are made in membrane regions of different thicknesses in the ratio of t_1:t_2, ranging from 1 to 3.75. Due to this geometrical difference in thickness, the pores have different ionic conductance and produce distinct current signals upon DNA translocation.

DEFINITIONS OF PORE DI METER ND THICKNESS

We define the membrane thickness, t, measured by ellipsometry after fabrication. For hourglass-shaped nanopores, the effective pore thickness, $t_{eff} = t/3$, fits well with the measured ionic conductance of TEM-drilled SiN pores.[21,23] This hourglass-shaped pore structure was previously confirmed by TEM tomography and is also consistent with measured conductance through our TEM-drilled SiN pores.[23–28] In conductance calculations, we assume a known pore thickness, constant over time and equal to 1/3 of the surrounding membrane thickness, which was shown to be a good assumption to model these pores over time.[20] The initial pore diameters, d, are measured from TEM images, corresponding to the smallest constriction region within the pore. The interpore distance, L, is observed under TEM and measured to be from the center of one pore to the center of the other.

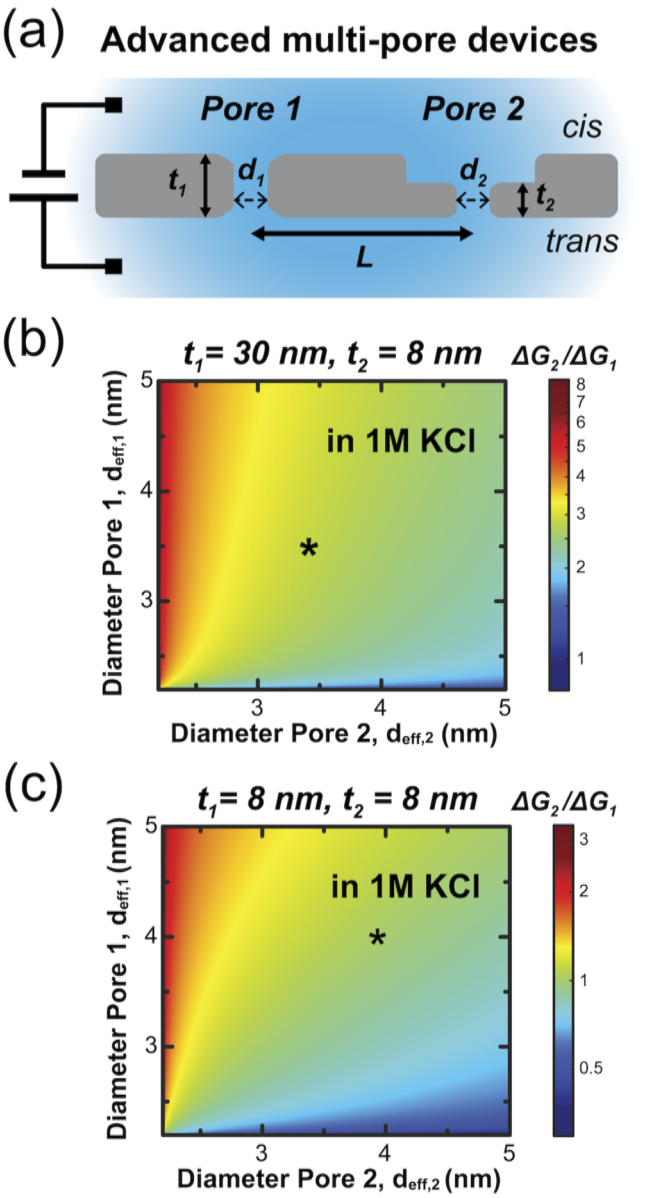

FIG 1. Schematic of two-pore devices and calculated conductance ratio upon dsDNA translocation. (a) Schematic of two nanopores on a suspended SiN membrane. Thickness and diameters for each nanopore are denoted as t_i and d_i (i = 1, 2), respectively, while the interpore distance, L, is defined from the center of d_1 to the center of d_2. dsDNA molecules are introduced from the *cis* chamber. [(b) and (c)] Color maps indicating the ratio of conductances, G_2/G_1, calculated via Eq. (2), as dsDNA blocks two nanopores with varying pore diameters denoted on the axes. The asterisk in (b) shows a ratio of blockage conductances of ~3 where $d_{eff,1} = d_{eff,2} = 3.5$ nm, while in (c) the asterisk indicates the ratio in blockage conductance drops to 1 as expected when the two pores are identical ($d_{eff,1} = d_{eff,2} = 4.0$ nm).

IONIC ME SUREMENTS

In preparation for ionic nanopore measurements, devices are treated with boiling piranha solution (1:3 v/v H_2O_2:H_2SO_4) to first

remove organic contamination from surfaces and to aid in pore wetting.[29] Followed by 10-min cleaning, devices are then rinsed with deionized (DI) water before being immersed in a TE buffer (10 mM Tris, 1 mM EDTA) 1 M KCl electrolyte solution (pH = 8.0, σ = 12.0 S/m) at room temperature. A VC100 amplifier (Chimera Instruments, New York, NY) records two-terminal ionic currents at 1 MHz, and an external bias voltage is applied via a set of Ag/AgCl electrodes.

NUMERIC L MODEL

To further strengthen our experimental findings, and in addition to simple equations, we perform a 3D simulation composed of Poisson–Nernst–Planck and Navier–Stokes equations with COMSOL Multiphysics (version 5.4).[30] The simulated system includes two individual nanopores drilled through the membrane connecting the two reservoirs (Fig. S1) in 1 M KCl solution. Two nanopores are cylindrical with different membrane thicknesses and are separated by a distance, L. To fit the data well, we use the effective thickness t_{eff} in the numerical modeling. The steric effect of ions[31] is taken into account in our modeling given that the pore size is relatively small. The surface charge density of the pore wall is assumed as 20 mC/m^2 at pH 8.0.[32–34] For simulating the current blockade from dsDNA translocation, we model DNA as a charged cylinder having 2.2 nm in diameter. A voltage bias of 200 mV is applied across the membrane to capture the DNA. The current blockade can be obtained numerically by changing the DNA positions along the axis through the pore's center and normal to the membrane.[35,36] Other details of the theoretical model are provided in the supplementary material.

OPEN PORE CURRENTS ND DN SIGN L CURRENTS

To analytically estimate the ionic current flowing through each open pore, I_i (where indices i = 1 and 2 denote pore 1 and pore 2), we use a cylindrical resistor model[37] of the pore surrounded by the top and bottom ionic hemispheres (access regions), where $R_{pore,i} = \frac{4t_{eff,i}}{\sigma\, {d_{eff,i}}^2}$, and including the contribution of the access regions, $R_{access,i} = \frac{1}{2\sigma d_{eff,i}}$, resulting in the pore conductance,

$$G_i = I_i/V_{bias} = \sigma\left(\frac{4t_{eff,i}}{{d_{eff,i}}^2} + \frac{1}{d_{eff,i}}\right)^{-1}, \tag{1}$$

where σ is the conductivity of solution, $t_{eff,i}$ is the effective nanopore thickness of each pore, and $d_{eff,i}$ is the effective nanopore diameter. The conductance change from the DNA translocating through one of the pores can be estimated by a cylindrical model as

$$G_i = \frac{I_i}{V_{bias}} = \sigma\left(\left[\frac{4t_{eff,i}}{d^2_{eff,i}} + \frac{1}{d_{eff,i}}\right]^{-1} \left[\frac{4t_{eff,i}}{\left(d^2_{eff,i} \quad d^2_{DNA}\right)} + \frac{1}{\sqrt{d^2_{eff,i} \quad d^2_{DNA}}}\right]^{-1}\right), \tag{2}$$

where V_{bias} is the applied transmembrane voltage and d_{DNA} is the cross-sectional width of DNA. In our case, we use double-stranded DNA with estimated d_{DNA} = 2.2 nm in Eq. (2). The signal, I, is maximized when the pore diameter approaches the width of DNA and when the nanopore thickness is minimized. The difference in pore geometries (e.g., pore diameters), illustrated in Fig. 1(a), provides a possibility to differentiate and analyze translocation events from different pores based on the ratio of measured conductances.

Figures 1(b) and 1(c) are color maps showing the expected ratio of dsDNA blockage conductance [$G_2/\ G_1$, derived by Eq. (2)] for two pores with thicknesses as seen in chip A (t_1 = 30 nm and t_2 = 8 nm) and chip B ($t_1 = t_2$ = 8 nm), where the axes denote the varying pore diameters. For pore diameters from 2 to 5 nm in chip A, the ratio of $G_2/\ G_1$ can be seen to vary from 1 to 8. For example, for a device with both pore diameters of 3.5 nm [asterisk marker in Fig. 1(b)], where one membrane thickness is 30 nm and the other is 8 nm, the conductance change from the thinner pore can be expected to be three times higher than that from the thicker pore. Alternatively, for chip B, the ratio of $G_2/\ G_1$ can only vary up to 3 when d_1 = 5 nm and d_2 = 2 nm.

High-resolution TEM images of chip A are shown in Fig. 2(a). Pore 1 (indicated with a blue arrow) is placed in the region where t_1 = 30 nm, and pore 2 (indicated with a yellow arrow) is placed within the locally thinned square region where t_2 = 8 nm. The interpore distance, L, is measured to be about 900 nm [Fig. 2(a), **left**]. Both pores are imaged under a higher magnification, and zoomed in TEM images are shown in insets of Fig. 2(a) (**middle** and **right**; the scale bar is 3 nm). Diameters d_1 and d_2 are measured in TEM to be about 3.5 nm, respectively. On the other hand, for the second design in chip B, both pore 1 and pore 2 are fabricated in locally thinned regions ($t_1 = t_2$ = 8 nm). The interpore distance for this chip is ~2 μm. Here, diameters d_1 and d_2 are measured in TEM to be about 4.0 nm [Fig. 2(b)].

In Table I, we note that the calculated and measured total conductances, G_{calc} (using the TEM-measured diameter and effective thicknesses) and G_{meas}, for the two devices are in close agreement (at day 0, 30.7 vs 31.2 nS for chip A; 52.6 vs 53.0 nS for chip B). Both devices have been measured right after drilling (day 0) and later (day 1 for chip A, day 11 for chip B), consecutively over several days [while being stored in ethanol:water (v:v 1:1) mixture in the freezer (18 °C)] in between the measurements, which was previously shown to preserve a constant pore diameter.[20] Over the course of consecutive I–V measurements on day 0, we notice that G_{meas} for chip A gradually increased from 31.2 to 41.4 nS after 3 h of measurement in 1 M KCl at applied bias up to 400 mV. This increase in conductance results from an increased pore diameter[20] from 3.5 nm (day 0) to about 4.3 nm (day 1) in chip A, and from 4 nm (day 0) to about 5.4 nm (day 11) in chip B. We note here the calculated pore resistances, R_{pore}, and access resistances, R_{access}, are as listed: for chip A, $R_{pore,1}$ = 57.4 MΩ and $R_{pore,2}$ = 15.3 MΩ, and $R_{access,1} = R_{access,2}$ = 9.7 MΩ; whereas for chip B, $R_{pore,1} = R_{pore,2}$ = 9.7 MΩ, and $R_{access,1} = R_{access,2}$ = 7.7 MΩ. Our previous work on the lifetime and stability of SiN pores[20] has shown that SiN nanopores expand over time in electrolyte solution with a similar diameter expansion rate (~1 nm/day in 1 M KCl at zero bias) for a range of thicknesses. Therefore, starting with similar diameters, $d_{TEM,i}$, for both pores, we assume $d_{eff,1} = d_{eff,2}$ throughout our calculation, which

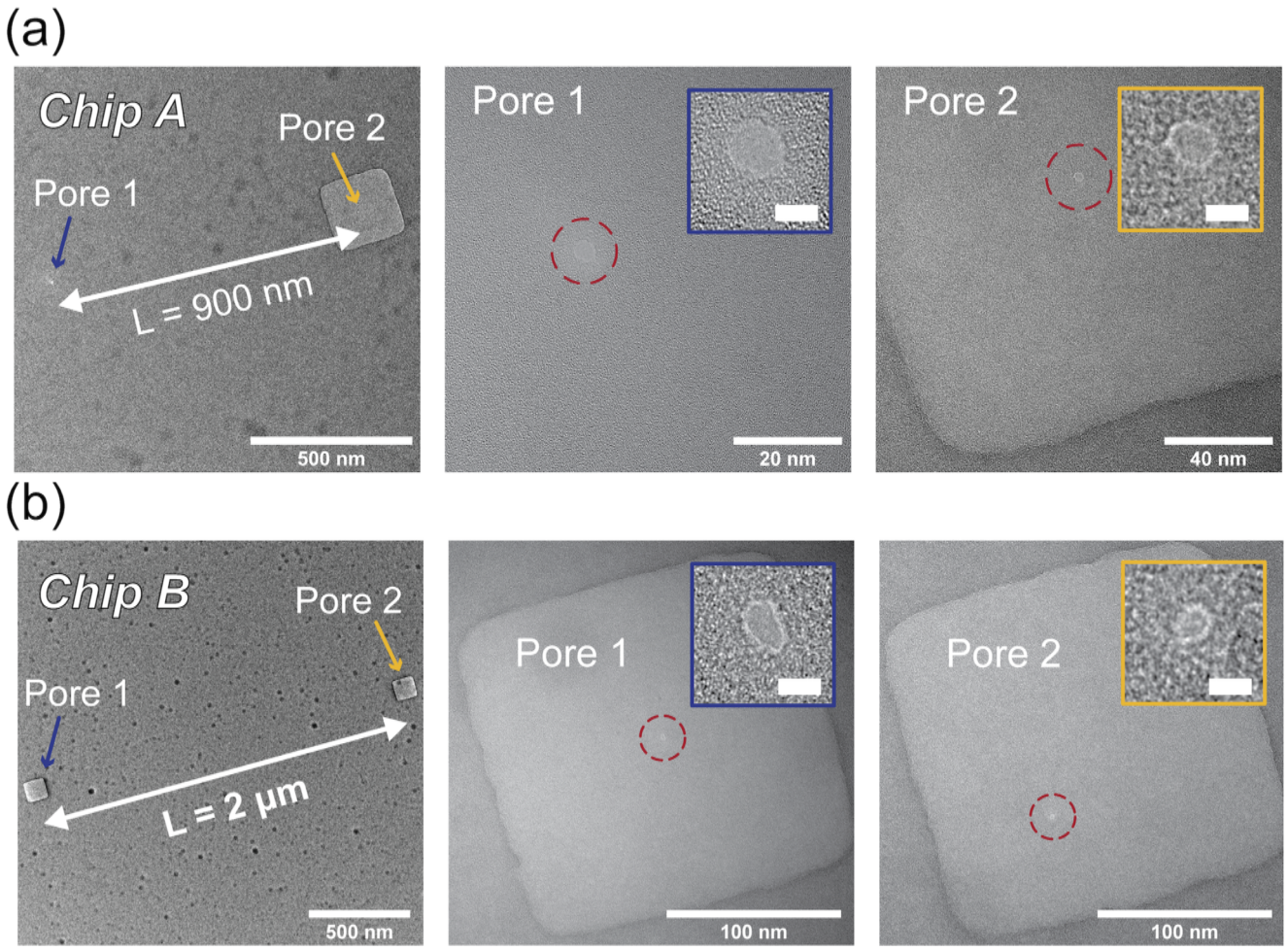

FIG 2. TEM images of chip A and chip B. (a) High resolution TEM images of chip A (left), where pore 1 (blue arrow) is drilled in a membrane region of thickness t_1 = 30 nm and pore 2 (yellow arrow) in a membrane region of thickness t_2 = 8 nm. The interpore distance L is 900 nm. Corresponding images of both nanopores are shown (middle and right). The red-dashed circles highlight the position of each pore; the insets are zoomed-in images of each pore (the scale bar is 3 nm). Diameters of pore 1 and pore 2 are approximately $d_1 = d_2 = 3.5$ nm. (b) High resolution TEM images of chip B (left) are labeled in a similar fashion, where the thickness of pore 1 (blue arrow) is changed to t_1 = 8 nm, while pore 2 (yellow arrow) stays at t_2 = 8 nm. The interpore distance L is measured to be about 2 μm. The insets are zoomed-in images of each pore, where the scale bar is 3 nm. From TEM images, the diameters for pore 1 and pore 2 are approximately $d_1 = d_2 = 4.0$ nm.

TABLE I. List of two-pore chip parameters for each pore, respectively. I–V measurements are conducted on day 0 for both chip A and chip B, day 1 for chip A, and day 11 for chip B. Note that all samples are measured in TE buffer (10 mM Tris, 1 mM EDTA) 1 M KCl under room temperature and ambient light (pH = 8.0, σ = 12.0 S/m). In between measurements, samples are rinsed with DI water and stored in a mixture solution of ethanol:water (v:v 1:1) at 18 °C.

		Pore1						Pore2									
Sample	Measurement timeline	$d_{TEM,1}$ (nm)	t_1 (nm)	$t_{eff,1}$ (nm)	$d_{eff,1}$ (nm)	$G_{calc,1}$ (nS)	$I_{calc,1}$ (nA)	$d_{TEM,2}$ (nm)	t_2 (nm)	$t_{eff,2}$ (nm)	$d_{eff,2}$ (nm)	$G_{calc,2}$ (nS)	$I_{calc,2}$ (nA)	V_{bias} (mV)	G_{calc} [a] (nS)	G_{meas} (nS)	$I_{0,meas}$ (nA)
Chip A	Day 0	3	30	10	3.5	9.1	1.8	3	8	2.6	3.5	21.6	4.3	200	30.7	31.2	6.2
	Day 1				4.3	13.0	2.6				4.3	28.8	5.8	200	41.8	41.4	8.3
Chip B	Day 0	3	8	2.6	4	26.3	2.6	4	8	2.6	4	26.3	2.6	100	52.6	53	5.3
	Day 11				5.4	39.8	4.0				5.4	39.8	4.0	100	79.5	78.9	7.9
							7.9						7.9	200			15.8

[a] $G_{calc} = G_{calc,1} + G_{calc,2}$.

TABLE II. Calculated event depths, I_{calc} (nA), at 200 mV for 8 possible dsDNA conditions (d_{DNA} = 2.2 nm) in the two-pore devices.

dsDNA condition (pore 1, pore 2)[a]	Calculated event depth, I_{calc} (nA)	
	Chip A	Chip B
(0, 0)	0.0	0.0
(u, 0)	0.7	1.4
(f, 0)	1.5	2.9
(0, u)	1.6	1.4
(0, f)	3.3	2.9
(u, u)	2.4	2.9
(u, f)	4.0	4.3
(f, u)	3.1	4.3
(f, f)	4.8	5.8

[a]u, unfolded DNA entry; f, folded DNA entry.

in turn matches well with measured conductances, where we see $G_{meas} \cong G_{calc} = G_{calc,1} + G_{calc,2}$.

The total conductance G of two pores of the same diameter d, at a distance L, was analytically derived by Gadaleta *et al*[19] and is given by the sum of conductance of two pores with a new diameter d , modified by an extra term $d/2L$,

$$G_{calc} = 2\sigma\left(\frac{4t}{d^2} + \frac{1}{d^2}\right)^{-1}, \quad (3)$$

where $d = \frac{d}{1+\frac{d}{2L}}$. Therefore, for our case $d \ll L$, $d \cong d$, the total open pore conductance is well-described by the sum of the individual pore conductances, G_1 and G_2, respectively.

With Eq. (2), we can calculate the corresponding current levels for each pore when dsDNA is passing through it in an unfolded (single-file) or folded (two-file) manner. Here, we introduce the following notation to indicate the blockage condition in both pores. Three indices are used to represent three possible DNA conditions: "0" is used to indicate no DNA is in the pore, while "u" and "f" are used to note that DNA is unfolded and folded in the pore, respectively. These indices are then filled into the bracket in the order as shown here (pore 1, pore 2), corresponding to the blockage status from each pore. For example, (u, 0) indicates a current level where dsDNA is in pore 1 unfolded, while pore 2 has no DNA, whereas (f, u) implies a folded DNA in pore 1 and an unfolded DNA in pore 2. Calculated event depths, including all eight possible DNA configurations in the pores, for chip A and chip B with V_{bias} = 200 mV are listed in Table II.

SIGNAL-TO-NOISE DEPENDENCE ON NANOPORE GEOMETRY

Measuring two nanopores with a two-terminal setup, a high signal-to-noise ratio (SNR) reading is crucial for efficient event detections. This is possible by engineering desired nanopore geometries, such as thickness and diameter, and by considering the noise in the system. To show the noise in these devices, in Fig. 3(a), we plot a 2.5-s-long concatenated open pore current trace, from chip B at

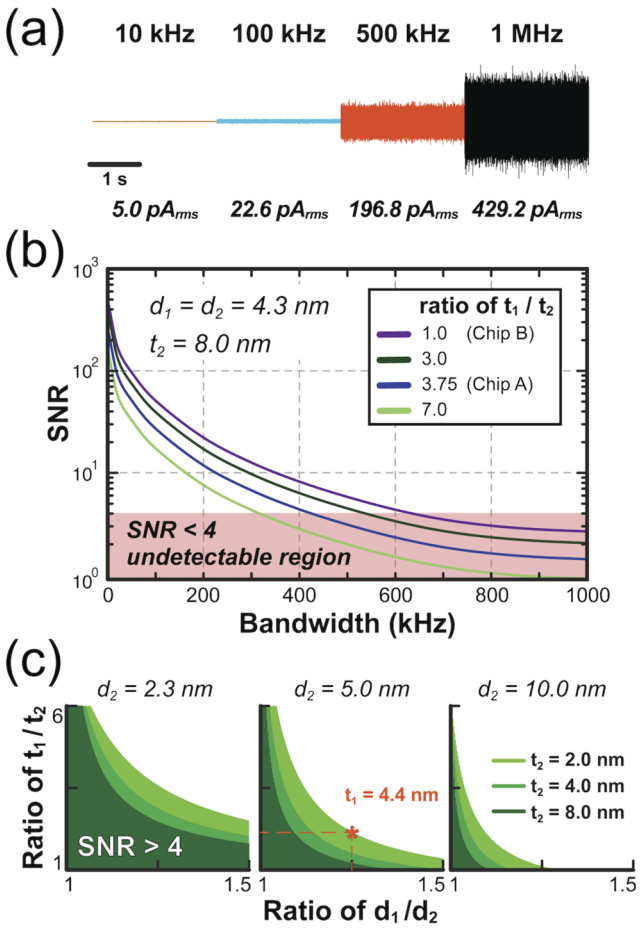

FIG 3. Open pore (baseline) rms noise, I_0^{rms}, of chip B and calculated signal-to-noise (SNR) ratio (I/I_0^{rms}) dependence on nanopore thickness and diameter. (a) Concatenated rms baseline current noise, I_0^{rms}, of a 2.5-s-long current trace at 0 mV in 1 M KCl (chip B). The trace is filtered using a digital four-pole Bessel filter to cutoff frequencies at 10 kHz, 100 kHz, 500 kHz, and 1 MHz, respectively. (b) Calculated SNR as a function of bandwidth using noise measurement from chip B. Four curves are presented for different nanopore thickness ratios, t_1/t_2 = 1.0, 3.0, 3.75, and 7.0, where fixed parameters are $d_1 = d_2$ = 4.3 nm and t_2 = 8.0 nm (chip B). The area highlighted in red indicates the region of the graph where SNR is below a threshold SNR of 4, for which events are difficult to detect. (c) Regions of SNR > 4 in green as a function of t_1/t_2 and d_1/d_2 for different values of fixed parameters d_2 and t_2. Three graphs are shown for three values of d_2 (= 2.3, 5.0, and 10.0 nm), each showing three regions of SNR > 4 corresponding to t_2 (= 2.0, 4.0, and 8.0 nm). Other parameters are the state (u, 0), cutoff frequency 100 kHz, with I_0^{rms} = 22.6 p $_{rms}$, d_{DN} = 2.2 nm, V_{bias} = 200 mV, and σ = 12.0 S/m. For d_2 = 5.0 nm and t_2 = 2.0 nm in the middle graph, if t_1 = 4.4 nm, to achieve SNR > 4, d_1 should be smaller than 6.25 nm.

0 mV, 1 M KCl, filtered at different frequencies. Specifically, the same trace is filtered via a digital four-pole Bessel filter at specific cutoff frequencies of 10, 100, 500, and 1 MHz with acquired I_0^{rms} equal to 5.0 pA_{rms}, 22.6 pA_{rms}, 196.8 pA_{rms}, and 429.2 pA_{rms}, respectively. The smallest possible I_0^{rms} that can be recorded with this experimental setup is 110 pA at 1 MHz, limited by the Chimera amplifier capacitance.[38] Here, we define the signal-to-noise ratio (SNR) = I/I_0^{rms} as

the ratio of the total current blockade in the two-pore chip, I (the sum of the current blockades from the two pores), and the measured input-referred current noise, I_0^{rms}, from Fig. 3(a).

To illustrate an approach how to engineer the two-pore system, given specific experimental constraints, we consider how the SNR depends on selected pore parameters. For example, in Fig. 3(b), we show the calculated SNR as a function of bandwidth (up to 1 MHz) for different thickness ratios t_1/t_2 = 1 (as in chip B), 3, 3.75 (as in chip A), and 7, where t_2 = 8 nm and $d_1 = d_2$ = 4.3 nm are fixed. We chose these specific values because they correspond to the thickness of the thinner pore (pore 2) and to the approximate pore diameters in chip A. In this example, to calculate I [Eq. (2)], we assume that unfolded dsDNA is in pore 1 and that there is no DNA in pore 2, corresponding to state (u, 0) (Table II). Other parameters used in Eq. (2) are d_{DNA} = 2.2 nm, V_{bias} = 200 mV, and σ = 12.0 S/m.

We see from Fig. 3(b) that as t_1/t_2 increases (t_2 is fixed to 8 nm), the SNR curves shift to lower values as expected as the thickness and resistance of pore 1 increase. Four SNR curves are shown: t_1/t_2 = 1.0 (t_1 = 8.0 nm), 3.0 (t_1 = 24.0 nm), 3.75 (t_1 = 30.0 nm), and 7.0 (t_1 = 56.0 nm). In order to detect events, we need a high enough SNR. We set this detection threshold to SNR = 4 (shown as the red region of SNR <4 in which events would not be easily detectable). From this, we see that the process of filtering events with cutoff frequencies above 300 kHz could lead to poor event identification, despite a higher temporal resolution. However, filtering events below this cutoff frequency could provide a sufficiently high SNR for event detection, yet a limited temporal resolution and accuracy in event structure. In other words, filtering at higher bandwidths, while providing the best possible time resolution, may miss the events altogether due to the increasing noise with increasing bandwidth.

To provide a more detailed picture of how SNR correlates with both the pore thickness and diameter, in Fig. 3(c), we plot regions of SNR > 4 (green), bounded by a curve of constant SNR of 4 as a function of t_1/t_2 (1–6) and d_1/d_2 (1–1.5) for different values of fixed parameters d_2 and t_2. Three graphs are shown for three values of d_2 (= 2.3, 5.0, and 10.0 nm), each showing three regions of SNR > 4 corresponding to three values of t_2 (= 2.0, 4.0, and 8.0 nm). Other parameters for SNR calculation here are the state (u, 0) as above, cutoff frequency 100 kHz, with $I_0^{rms} = 22.6\ pA_{rms}$, d_{DNA} = 2.2 nm, V_{bias} = 200 mV, and σ = 12.0 S/m. For instance, in the middle graph, assuming d_2 = 5.0 nm and t_2 = 2.0 nm, if the thickness of pore 1 is set to t_1 = 4.4 nm, to achieve SNR > 4, the diameter of pore 1, d_1, should be smaller than 6.25 nm.

RESULTS ND DISCUSSION

For the data represented in Fig. 4(a) (day 1), chip A (t_1 = 30 nm, t_2 = 8 nm, $d_1 = d_2$ = 4.3 nm) is measured with V_{bias} = 200 mV in 1 M KCl. We show a 5 kbp dsDNA (200 nM, NoLimits 5000 bp DNA Fragments, ThermoFisher Scientific) translocation current trace recording at 1 MHz bandwidth over a total duration of 120 s, filtered down using a four-pole Bessel filter at 100 kHz. A total of N = 12 406 qualified events are detected by choosing a 4σ threshold (SNR = 4), where $\sigma = I_0^{rms}$. The all-points histogram (plotted with data acquired at 1 MHz and digitally filtered at 100 kHz) of this trace is shown below the trace on the left, where we observe a multiple-peak current distribution over a wide range of currents (from 3.8 to 9.1 nA). We then obtain the following values from the apparent peak current positions: The red solid line is located at 8.3 nA, the yellow dashed line is located at 7.5 nA, the green dashed line is located at 6.8 nA, and the orange dashed line is located at 5.0 nA. A 1-s-long subset of this long current trace (highlighted in light blue) is zoomed in and provides a more detailed view of the high quality of the current recording. In conjunction with the calculation result shown in Table II, the current peak positions acquired from all-points histogram give us a glimpse into the corresponding translocation event compositions. For instance, the event depth (u, 0) when unfolded DNA goes through pore 1 is calculated to be 0.7 nA, which matches well with the experimental value of 0.8 nA. However, a peak position of 6.8 nA (yellow dashed line) could correspond to either one folded DNA passing through pore 1 or an unfolded DNA passing through pore 2 since the estimated event depth levels for (f, 0) = 1.5 nA and (0, u) = 1.6 nA are relatively close, requiring further event analysis, to distinguish unfolded DNA events (single-file) from folded DNA events (two-file). As shown in Table I, the effective diameters, $d_{eff,1}$ and $d_{eff,2}$, are calculated to be 4.3 nm, which sits at the tipping point of allowing the passage of folded dsDNA with a diameter of 4.4 nm. In addition, the absence of any other clearly distinguishable peaks in the histogram implies that other states, such as (u, f) and (f, f) when two DNA molecules are in both pores at the same time and the total current blockade is maximal, are less likely to occur, although there are points in the histogram that could correspond to these estimated event levels [Fig. 4(a)], which will be discussed later.

In contrast, translocation data characteristics from two pores of similar thickness and diameters on the same chip and using the same DNA are very different. We show translocation recordings (day 11) in Fig. 4(b), acquired from chip B ($t_1 = t_2$ = 8 nm, and calculated diameters $d_1 = d_2$ = 5.4 nm) with V_{bias} = 100 mV and 1 kbp dsDNA fed into the *cis* chamber. A current trace and the all-points histogram of a 60-s-long trace are shown. Under the same conditions, we observe, in contrast, a relatively narrow current distribution over the current range from 6.2 to 8.3 nA. From the histogram, we acquire the current peak positions, labeled by the red solid line, indicating the baseline open pore current when both pores are open, at 7.9 nA and the pink dashed line at 7.1 nA. This is equivalent to an event depth of 0.8 nA, in good agreement with the calculated event depth of 0.7 nA corresponding to unfolded DNA passing through either pore, scenarios labeled as (u, 0) and (0, u) in Fig. 4(b). We observe a relatively narrow distribution of currents in the all-points histogram [Fig. 4(b), left], owing to the fact that this device consists of two nanopores that are almost identical (with the same nominal thickness and diameter). Provided that the same analyte is detected, each of the two pores will record a similar event depth, e.g., (0, f), (f, 0), and (u, u) would all share the same event depth level at 2.9 nA. Here, the event depth corresponding to a folded (two-file) event is estimated from Eq. (2) by assuming that two dsDNA cross-sectional areas block the pore.

Event identification and their quoted number depend on the measurement bandwidth and filtering cutoff frequency, event thresholds, and other parameters. We show how both all-points histograms in Figs. 4(a) and 4(b) evolve for different filtering frequencies up to 1 MHz in the supplementary material (Figs. S4 and S5).

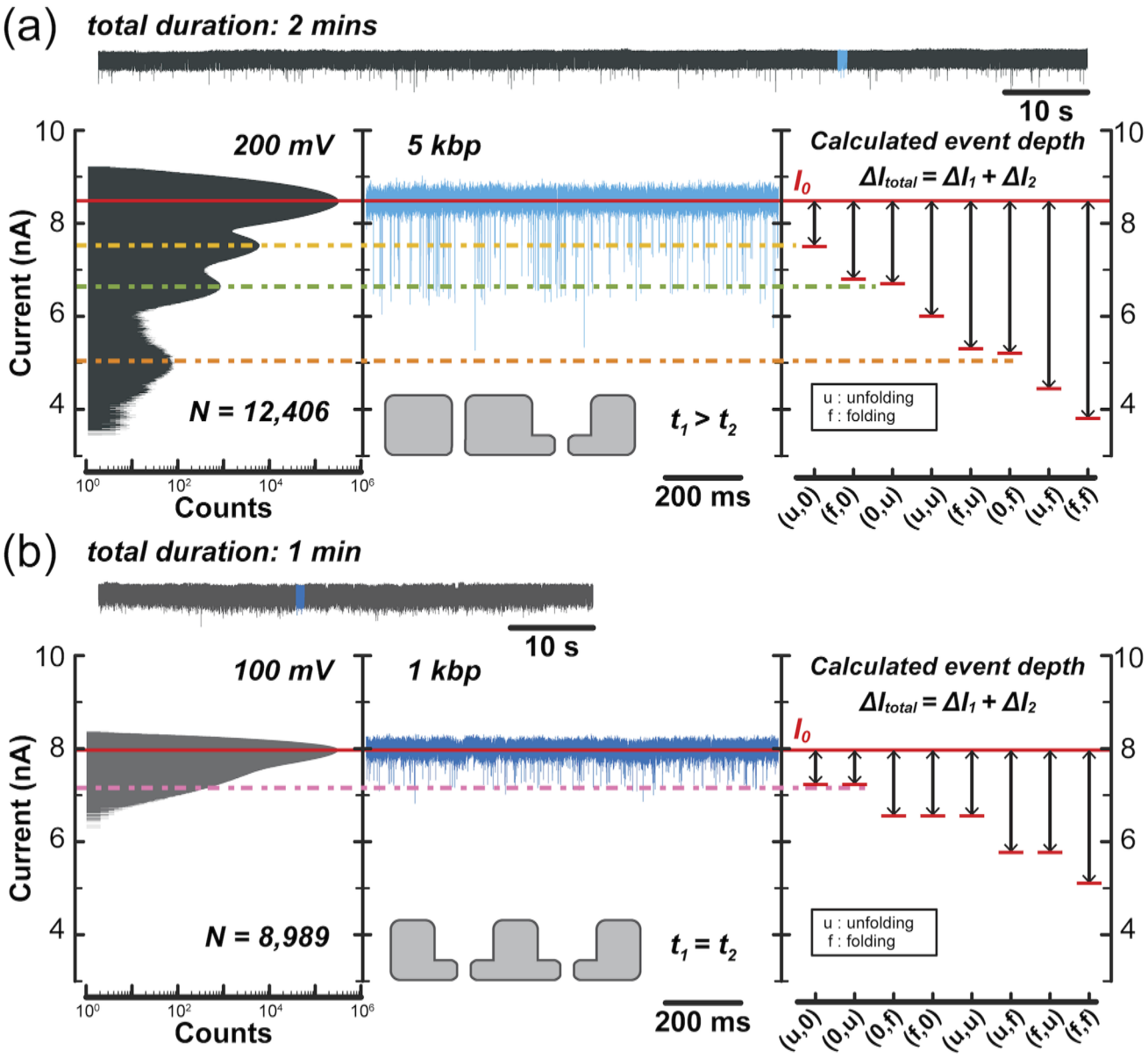

FIG 4. Analysis of dsDNA translocation data in two-pore devices. (a) Complete current trace from 5 kbp dsDNA translocation at 200 mV from chip A with total duration of 120 s and a total detected number of events N = 12 406. The all-points histogram (left) indicates a multiple-peak current distribution. A zoomed-in section of the current trace with 1 s duration (blue, middle) is shown. The peak positions are at 8.3 nA (red), 7.5 nA (yellow), 6.8 nA (green), and 5.0 nA (orange). These levels are in concordance with calculated event depths (left), (u, 0) and (0, u). (b) Complete current trace of 1 kbp dsDNA translocation at 100 mV from chip B with a total duration of 60 s and a total detected number of events N = 8989. The all-points histogram (left) indicates a bimodal current distribution. A zoomed-in section of the current trace with 1 s duration (blue, middle) is shown. The peak positions are at 7.9 nA (red) and 7.1 nA (pink), which agree with calculated event depths (left) of (u, 0) and (0, u). On the right, we label the position of the missing levels, e.g., (0, f), and (u, u).

At higher filtering frequencies, the peaks are gradually lost as more data points are included and the noise increases, which results in a shift of characteristic dwell time, τ, toward shorter time.[39] The main advantage of filtering at higher frequencies is that very short events can be detected, which might be otherwise missed at lower filtering frequencies or have their current amplitudes underestimated. Such aspects of event detection and optimization depending on which classes of events are being analyzed have been previously discussed in detail by Rosenstein *et al*.[40] who showed the first recordings up to 1 MHz[40] and up to 5–10 MHz detection by Shekar *et al*.[39] and Chien

et al,[41] as well as Wanunu *et al* who developed silicon nitride pore thinning below 10 nm[21] for detection of short molecules and short events.

To further trace each detected event back to one of the two pores, we implement a data analysis method to categorize events into different groups. We observe three broad groups based on the shape of the current pulse: One-step (rectangular pulse) events are categorized as type I, two-step events are categorized as type II, and multiple-step events are categorized as type III. In the first row of examples in Fig. 5(a), we showcase sample events from these groups detected from chip A. For type I events, we can distinguish clearly between (u, 0) = 0.7 nA and (0, u) = 1.6 nA. For type II events, the partially folded events (with two current levels inside of the events) have their own signature steps between a folded state and an unfolded state. We are able to label these substructures within events and attribute them to the corresponding pore through which

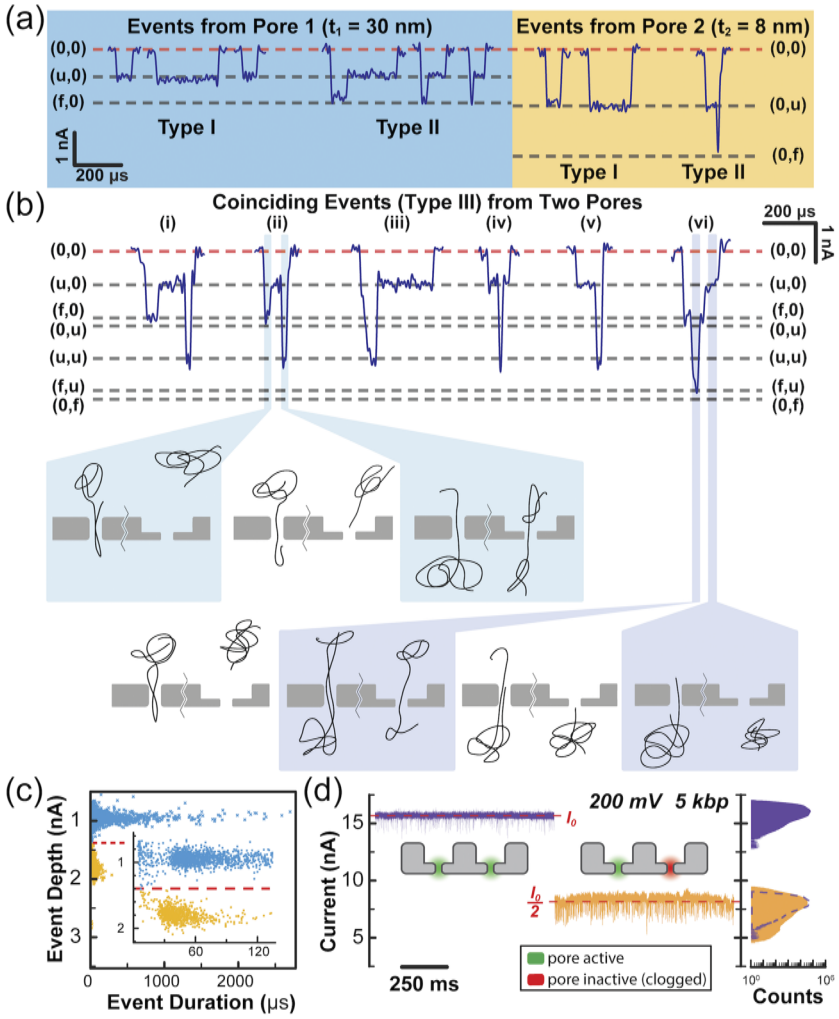

FIG 5. Event analysis of dsDNA translocation data from two-pore devices. (a) Sample events from data filtered at 100 kHz from pore 1 (t_1 = 30 nm) and pore 2 (t_2 = 8 nm), respectively. Distinctive current level steps, due to pore thickness differences, aid in categorizing events with one-step (type I) and two-steps (type II) and attributing them to one of the two pores. (b) Six example "coinciding" events from data filtered at 100 kHz from chip A where additive event depths, up to ~40 total blockade, indicate simultaneous dsDNA translocation through the two separate pores. Detailed DNA translocation illustrations are proposed underneath as the likely interpretations for events (ii) and (vi), where specific sections of each signal correspond to a specific snapshot of the proposed event progression. (c) Scatter plot for chip A type I (one-step) events showing event durations vs event depths. Two spread out data distributions indicate data from the two pores. The top dataset (blue) has a median event depth of 0.95 0.08 nA, indicating unfolded dsDNA events in pore 1, (u, 0); the bottom dataset (yellow) has a median depth of 1.80 0.10 nA with closely matching the expected unfolded current level in pore 2, (0, u). The inset shows a closer view of both datasets and event durations, where the characteristic dwell time, τ, from the top dataset is at ~132 μs, while the bottom dataset is at ~88 μs. (d) Concatenated current trace of 5 kbp dsDNA translocation at 200 mV from chip B where both pores open/active (purple) and only one of the pores is active (orange). Each trace has a 1-s duration. When one of the pores is fully blocked (clogged) by the DNA, the current baseline is halved and fluctuates with a higher I_0^{rms}. All-points histograms from both traces are shown, and the purple dashed outline is used to compare the current distributions for the two-pore active state (purple solid) and the one-pore active state (orange solid).

DNA passes. The dashed gray lines in Fig. 5, which correspond to calculated current blockades (Table II), match well with the measured values. With events produced from pore 1 (t_1 = 30 nm), we expect the deep step to be at a current level of (f, 0) = 1.5 nA, while the shallow step at (u, 0) = 0.7 nA. In contrast, a partially folded dsDNA entering through pore 2 (t_2 = 8 nm) would produce a step-like event with deep and shallow current levels at (0, f) = 3.3 nA and (0, u) = 1.6 nA, respectively.

In our work, the individual DNA molecules are too short compared to the interpore distance to span both pores at the same time. In contrast, Pud *et al*[14] measured 10–50 times longer dsDNA than what is used in our work and claimed molecule's mechanical trapping by the two pores by observing some very long events. Their pores were drilled in 20-nm-thick SiN with pore diameters of 10 and 16 nm and separated by ~100 nm to 1 μm. A sample containing 48 kbp (16.3 μm) dsDNA in 2M LiCl was used, and in this case, the DNA was more than 10 times longer than the interpore separation. Because of this, the authors claimed that some of the observed long-duration events, as compared to the typical durations of regular translocation events, can be interpreted to correspond to the DNA strand threading with its two ends through both pores at the same time.[14]

COINCIDING EVENTS

One of our unique findings with DNA translocations via two pores is when two dsDNA molecules interact with both pores individually and concurrently, producing an overall event that consists of two events through each pore that overlap in time. We have observed that ~0.7 of the total number of events could be attributed to these coinciding events, 93 out of N = 12 406 total events detected from chip A. The measured current pulse from the two-pore chip is then composed of two single-pore signals that are additive (expected, as seen with open pore $G = G_1 + G_2$). Despite being two-terminal signals, they allow for precise insight into how dsDNA interacts with each pore and the device as a whole. In other words, one current trace with composite events can be deconstructed into two traces corresponding to each pore with high fidelity because the pores have significantly different thicknesses. Figure 5(b) demonstrates examples of coinciding events with 5 kbp dsDNA under 200 mV bias in chip A. Six selected events are labeled (i) through (vi) in Fig. 5(b). Underneath, we show the pictorial illustrations of the most likely translocation scenarios happening in the two pores based on corresponding current levels within some events. For example, based on the current levels within event (i), this event can be interpreted as follows: One dsDNA molecule first enters the thick pore with its end folded, resulting in an (f, 0) current level. The dsDNA then unfolds in the pore, resulting in a (u, 0) current level. While the dsDNA is still translocating unfolded through the thick pore, second dsDNA strand passes through the thinner pore unfolded, which brings the current level down to (u, u). Once the second dsDNA has exited the thin pore, the current briefly rises back up to (u, 0) where the remainder of the first dsDNA in the thick pore exits, and then the current returns to the baseline, (0, 0). Event (ii) is similar to event (i) and is illustrated in Fig. 5(b), except that the dsDNA molecules exit both pores at similar times. Events (iii) through (v) could be interpreted as composite events where an unfolded dsDNA passes through the thick pore and another unfolded dsDNA passes through the thin pore sometime during the event recorded in the thick pore [at the beginning, in the middle, or at the end of the event, shown in events (iii), (iv), and (v)]. This brings the current briefly from (u, 0) to (u, u). In event (vi), as shown in the sequence of diagrams in Fig. 5(b), dsDNA first passes folded through the thick pore, producing an (f, 0) current level. While the first dsDNA stays folded in the thick pore, another dsDNA molecule passes quickly through the thin pore unfolded, producing the (f, u) current level briefly, until the DNA event in the thin pore has ended and the current goes back to the (f, 0) level. Finally, the dsDNA exits the thick pore unfolded, resulting in the (u, 0) level.

There are a few considerations to note involving the coinciding events outlined above for an asymmetric two-pore device. A close examination into coinciding event steps is required in order to exclude the less likely interpretations of how DNA molecules enter both pores, especially when different scenarios can produce similar current levels. For example, in the case of chip A, where (f, 0) = 1.5 nA and (0, u) = 1.6 nA, a folded strand of dsDNA in the thick pore could produce a similar signal as an unfolded dsDNA translocating through the thin pore. For event (i), besides the explanation provided earlier involving two strands of dsDNA, another plausible interpretation would be the following: one unfolded DNA passing through the thin pore, (0, u), and as soon as the first strand exits, a second strand consecutively enters into the thick pore unfolded, (u, 0), which is then followed by a third strand of unfolded DNA translocating through the thin pore, (u, u). The later interpretation would be deemed less likely since three strands are involved.

The scatter plot of type I (rectangular shape) events from chip A showing event durations vs event current depths is featured in Fig. 5(c). We observe two distinctly separated sets of data points. Based on the event current depth median, we are able to identify and assign the top set (in blue) to events originating from pore 1 (t_1 = 30 nm) with a median event current depth of 0.95 ± 0.08 nA, while the bottom dataset (in yellow) showing a median of 1.80 ± 0.10 nA, to events through pore 2 (t_2 = 8 nm). The separation line drawn (red-dashed line) to divide the top dataset from the bottom one is chosen to be the average value between the two medians, about ~1.38 nA. This separation of events, assuming a high enough signal-to-noise ratio, opens a gateway for future nanopore engineering to achieve parallel reading without the necessity for multiple electrode designs. Moreover, we also observe a difference in event durations, τ, where the characteristic dwell time for the top dataset is ~132 μs, while it is ~88 μs for the bottom set. The dwell time distribution is well represented by an exponential decay function ($e^{-t/\tau}$). With a fixed voltage for unfolded DNA molecules, analytes will experience a similar pulling force from one chamber (*cis*) to the other (*trans*). The geometrical thickness of the nanopore and the length of the DNA affect how long the ionic blockage lasts. Previously published results[21] showed a ~30 decrease in dwell time when comparing translocating 3 kbp dsDNA through two individual single nanopores with a thickness ratio of 1:10 (6 and 60 nm, respectively). In adddition, the event duration is reported to be governed by separate power laws depending on the length of DNA.[42] Given a 5 kbp dsDNA with a pair of two nanopores with a thickness ratio of 8:30 = 1:3.75, we see a ratio of 1:1.5 in the characteristicdwell

time, i.e., a decrease of ~33% in event duration as pore decreases in thickness by ~73%.

We can also record translocations directly from one pore when the counterpart nanopore is clogged, i.e., fully blocked for a prolonged period of time. This example is given by the current trace from chip B ($t_1 = t_2 = 8$ nm) with 5 kbp dsDNA at 200 mV. At the beginning of the measurement, the total open pore current is coming from both pores, $I_0 = 15.8$ nA, consistent with both pore 1 and pore 2 being open. As one of the pores clogs, the open pore current drops to approximately half of the initial value, 7.8 nA ~ $I_0/2$, since the two pores are almost identical. The red dashed lines in Fig. 5(b) are the calculated open pore currents (I_0 and $I_0/2$) that match well with the experimental values. Furthermore, the baseline noise is visibly higher when one of the pores is clogged by the DNA, compared to the case when both pores are open. Examples of concatenated 1-s-long current traces from chip B before and after one-pore-clogging are shown in Fig. 5(d). All-points histograms from these two traces show a widening wing in the histogram corresponding to one of the pores being clogged (orange), compared to the case when both pores are open and active (purple). This widening of the histogram correlates well with the degree of current baseline fluctuation in both cases. I_0^{rms} before and after the clogging are measured and show a ~16% increase from ~600 pA_{rms} to ~700 pA_{rms}.

FUTURE WORK

Given our two-pore results presented here, future studies focusing on the higher complexity parallel reading systems could be achieved with advanced nanofabrication processes. For example, one could conceptually consider making an array of N pores with a range of thicknesses (with fixed or varying diameters). To fabricate such multiple-thickness nanopore devices within a single SiN membrane, it may be necessary to repeat EBL patterning/thinning steps, where precise alignments between each e-beam lithography exposure/patterning cycle is needed. Varying pore diameters only (while keeping a constant pore thickness) is experimentally much simpler since all pores would be drilled in one TEM step. For practical considerations, we note that our fabrication yield here was 70% (this is the percentage of devices where we successfully thinned the membrane from 30 to 8 nm without its perforation by RIE dry etching). After the devices were fabricated, a stable open pore current served as a key factor indicating how reliable translocation data recordings and event analysis were.

OTHER PRACTICAL CONSIDERATIONS: YIELD OF SILICON NITRIDE NANOPORES THAT GIVE STABLE IONIC CURRENT

With standardized wetting and cleaning procedures for TEM-drilled silicon nitride nanopore devices[43] used in our experiments, we observed an ionic performance yield (percentage of devices that gave stable ionic current consistent with Eq. (1) and the measured nanopore size) of 73% for single-pore devices used as controls (statistics out of 11 chips), much similar to the previously reported result[44] and our lab's past experiences. In other words, the percentage of such well-performing silicon nitride nanopores for DNA translocations is high. For two-pore devices, we obtained an ionic performance yield of 66% (percentage of two-pore devices where the ionic current from both pores was stable and equal to the calculated value based on measured pore dimensions).

SCALING TO MORE THAN TWO PORES

Now, for the purpose of speculation, consider a case where the number of pores on a chip was to increase to an arbitrary value N. We would expect that the number of N-pore devices where all pores are conducting is $(0.73)^N$. For $N = 2$, this is 53%, a bit lower than what we observed, 66%. For $N = 10$, we would then expect 4% of devices to have all ten pores conducting on a single SiN membrane chip. In other words, to have a device with 10 pores conducting, we may need to fabricate 250 pores on one device on average. While this kind of analysis is a useful theoretical exercise in considering future potential of scaling up, we note that higher yield estimates are possible, by considering, for example, ~1 nm-thick-HfO_2 coated silicon nitride pores that were shown to be more stable.[20] Another possible modification that could aid in a high fabrication yield is implementing electron-based local SiN membrane thinning via STEM.[24] With real time EELS signal reading, we can precisely control the thinning of multiple membrane regions to various desired thicknesses.

In addition to experimental yields discussed above, the possible number of pores on a chip that could produce distinguishable ionic current levels depends on many other parameters. The SNR is a crucial parameter, and while it is already high in this work, it can be improved, e.g., by using lower capacitance chips to reduce noise to the minimum.[41] Amplifier improvements will also help us to achieve high SNR readings. In other words, the possibility of scaling depends not only on the nanopore dimensions and properties but also the overall device designs and electronic setup architecture. Depending on the specific experiment, the choice of pore diameters and thicknesses could also be partially informed by the modeling in Fig. 3(c) and Eq. (2) for a specific analyte. To illustrate this, here we demonstrate examples in fixing diameters and thicknesses separately for ssDNA. From the analysis shown above in Figs. 5(a) and 5(b), we are able to distinguish difference in event depth as small as 0.1 nA, given the ionic current is stable and clear over time. Here, we consider translocating ssDNA ($d_{DNA} = 1.2$ nm) in 1 M KCl with both pore diameters fixed to be $d_1 = d_2 = 1.4$ nm[41] and $t_2 = 8$ nm. In this case, we would expect to distinguish levels from two pores with thickness difference, t, as small as 1 nm ($t_1 = 9$ nm). The calculated event depths for ssDNA blocking conditions (u, 0) and (0, u) are 0.3 and 0.4 nA at 200 mV. On the other hand, if we fixed $t_1 = t_2 = 8$ nm and $d_2 = 1.4$ nm, while altering the other pore diameter to $d_1 = 1.6$ nm, the corresponding calculated event depths for (u, 0) and (0, u) would be distinguishable (1.3 and 1.4 nA). However, if we further decrease the differences either in thickness $t < 1$ nm or in diameter $d < 0.2$ nm, it might be challenging to differentiate events from one pore to another under these experimental setup conditions. For a given analyte to be detected, the important parameters to be adjusted include pore dimensions (diameter, thickness) and the device and amplifier capacitances that affect SNR.[38,39,41]

CONCLUSION

In this work, we made devices with two nanopores in parallel, where the nanopores are of diameters comparable to the width of dsDNA but have different ratios of thicknesses, in order to produce similar or distinctly different open pore and DNA translocation signals. The pores are relatively far away from each other compared to the nanopore diameter, $L \gg d$, and we prove that the total conductance of a two-pore chip is the sum of the conductances from each individual nanopore. Since the pores produce distinct conductances, we are able to monitor signals with a two-terminal measurement and evaluate whether both, one, or no pores are actively open and conducting. In addition, we are able to analyze and categorize the DNA signals from each pore based on specific event current depths produced by each pore. We also observe a few different types of "coinciding" events where two DNA molecules pass through the two pores at approximately the same times and the total current blockage goes to ~40 . Finally, this approach may be generalizable to devices with more than two different pores (and also different analytes) where individual signals can be targeted and extracted from a conventional two-terminal measurement.

SUPPLEMENT RY M TERI L

See the supplementary material for a numerical model on two-pore devices and all-points histogram and scatter plot evolution, demonstrated over various cutoff frequencies.

UTHORS' CONTRIBUTIONS

Y.-C.C., and M.D. conceived the project idea. Y.-C.C. fabricated devices for ionic measurements and performed TEM imaging and analysis. J.C. conducted translocation data analysis. C.-Y.L. conducted COMSOL work. The manuscript was written through contributions of all authors. All authors have given approval to the final version of the manuscript.

CKNOWLEDGMENTS

This research was primarily supported by the NIH (Grant No. R21 HG010536) and by the NSF (Grant No. EFRI 2-DARE 1542707) (participant fund for undergraduate research). This work was performed, in part, at the University of Pennsylvania's Singh Center for Nanotechnology, an NNCI member supported by NSF Grant No. ECCS-1542153. We thank Dr. Douglas Yates and Dr. Hiromichi Yamamoto at the University of Pennsylvania for generous help with TEM and EBL.

The authors declare the following competing financial interest(s): M.D. is a consultant and founder of Goeppert (www.gppert.com), which manufactures nanotechnology-related products including solid-state nanopore chips and 2D membranes.

D T V IL BILITY

The data that support the findings of this study are available from the corresponding author upon reasonable request.

REFERENCES

[1] L. Xue, H. Yamazaki, R. Ren, M. Wanunu, A. P. Ivanov, and J. B. Edel, Nat. Rev. Mater. **5**, 931 (2020).
[2] G. Danda and M. Drndić, Curr. Opin. Biotechnol. **55**, 124 (2019).
[3] K. Healy, B. Schiedt, and A. P. Morrison, Nanomedicine **2**, 875 (2007).
[4] D. Branton, D. W. Deamer, A. Marziali, H. Bayley, S. A. Benner, T. Butler, M. Di Ventra, S. Garaj, A. Hibbs, X. Huang, S. B. Jovanovich, P. S. Krstic, S. Lindsay, X. S. Ling, C. H. Mastrangelo, A. Meller, J. S. Oliver, Y. V. Pershin, J. M. Ramsey, R. Riehn, G. V. Soni, V. Tabard-Cossa, M. Wanunu, M. Wiggin, and J. A. Schloss, Nat. Biotechnol. **26**, 1146 (2008).
[5] D. Deamer, M. Akeson, and D. Branton, Nat. Biotechnol. **34**, 518 (2016).
[6] D. W. Deamer and M. Akeson, Trends Biotechnol. **18**, 147 (2000).
[7] C. Dekker, Nat. Nanotechnol. **2**, 209 (2007).
[8] K. Briggs, G. Madejski, M. Magill, K. Kastritis, H. W. de Haan, J. L. McGrath, and V. Tabard-Cossa, Nano Lett. **18**, 660 (2018).
[9] M. H. Lam, K. Briggs, K. Kastritis, M. Magill, G. R. Madejski, J. L. McGrath, H. W. de Haan, and V. Tabard-Cossa, ACS Appl. Nano Mater. **2**, 4773 (2019).
[10] X. Liu, Y. Zhang, R. Nagel, W. Reisner, and W. B. Dunbar, Small **15**, 1901704 (2019).
[11] X. Liu, P. Zimny, Y. Zhang, A. Rana, R. Nagel, W. Reisner, and W. B. Dunbar, Small **16**, 1905379 (2020).
[12] Y. Zhang, X. Liu, Y. Zhao, J.-K. Yu, W. Reisner, and W. B. Dunbar, Small **14**, 1801890 (2018).
[13] P. Cadinu, G. Campolo, S. Pud, W. Yang, J. B. Edel, C. Dekker, and A. P. Ivanov, Nano Lett. **18**, 2738 (2018).
[14] S. Pud, S.-H. Chao, M. Belkin, D. Verschueren, T. Huijben, C. van Engelenburg, C. Dekker, and A. Aksimentiev, Nano Lett. **16**, 8021 (2016).
[15] M. Langecker, D. Pedone, F. C. Simmel, and U. Rant, Nano Lett. **11**, 5002 (2011).
[16] D. Pedone, M. Langecker, G. Abstreiter, and U. Rant, Nano Lett. **11**, 1561 (2011).
[17] D. Pedone, M. Langecker, A. M. Münzer, R. Wei, R. D. Nagel, and U. Rant, J. Phys.: Condens. Matter **22**, 454115 (2010).
[18] P. Xie, Q. Xiong, Y. Fang, Q. Qing, and C. M. Lieber, Nat. Nanotechnol. **7**, 119 (2012).
[19] A. Gadaleta, C. Sempere, S. Gravelle, A. Siria, R. Fulcrand, C. Ybert, and L. Bocquet, Phys. Fluids **26**, 012005 (2014).
[20] Y.-C. Chou, P. Masih Das, D. S. Monos, and M. Drndić, ACS Nano **14**, 6715 (2020).
[21] M. Wanunu, T. Dadosh, V. Ray, J. Jin, L. McReynolds, and M. Drndić, Nat. Nanotechnol. **5**, 807 (2010).
[22] K. Venta, G. Shemer, M. Puster, J. A. Rodríguez-Manzo, A. Balan, J. K. Rosenstein, K. Shepard, and M. Drndić, ACS Nano **7**, 4629 (2013).
[23] M. J. Kim, B. McNally, K. Murata, and A. Meller, Nanotechnology **18**, 205302 (2007).
[24] J. A. Rodríguez-Manzo, M. Puster, A. Nicolaï, V. Meunier, and M. Drndić, ACS Nano **9**, 6555 (2015).
[25] G. Madejski, K. Lucas, F. C. Pascut, K. F. Webb, and J. L. McGrath, Membranes **8**, 26 (2018).
[26] C.-H. Chen, X. Chang, and C.-S. Wu, Sci. Rep. **9**, 18663 (2019).
[27] M. van den Hout, A. R. Hall, M. Y. Wu, H. W. Zandbergen, C. Dekker, and N. H. Dekker, Nanotechnology **21**, 115304 (2010).
[28] M.-Y. Wu, R. M. M. Smeets, M. Zandbergen, U. Ziese, D. Krapf, P. E. Batson, N. H. Dekker, C. Dekker, and H. W. Zandbergen, Nano Lett. **9**, 479 (2009).
[29] M. Wanunu and A. Meller, Nano Lett. **7**, 1580 (2007).
[30] C.-Y. Lin, E. Turker Acar, J. W. Polster, K. Lin, J.-P. Hsu, and Z. S. Siwy, ACS Nano **13**, 9868 (2019).
[31] M. S. Kilic, M. Z. Bazant, and A. Ajdari, Phys. Rev. E **75**, 021503 (2007).
[32] M. Firnkes, D. Pedone, J. Knezevic, M. Döblinger, and U. Rant, Nano Lett. **1** , 2162 (2010).

[33]S. Mezzasalma and D. Baldovino, J. Colloid Interface Sci. **18** , 413 (1996).
[34]C. Ho, R. Qiao, J. B. Heng, A. Chatterjee, R. J. Timp, N. R. Aluru, and G. Timp, Proc. Natl. Acad. Sci. U. S. A. **1 2**, 10445 (2005).
[35]S. van Dorp, U. F. Keyser, N. H. Dekker, C. Dekker, and S. G. Lemay, Nat. Phys. **5**, 347 (2009).
[36]Y. He, M. Tsutsui, C. Fan, M. Taniguchi, and T. Kawai, ACS Nano **5**, 5509 (2011).
[37]S. W. Kowalczyk, A. Y. Grosberg, Y. Rabin, and C. Dekker, Nanotechnology **22**, 315101 (2011).
[38]A. Balan, B. Machielse, D. Niedzwiecki, J. Lin, P. Ong, R. Engelke, K. L. Shepard, and M. Drndić, Nano Lett. **14**, 7215 (2014).
[39]S. Shekar, D. J. Niedzwiecki, C.-C. Chien, P. Ong, D. A. Fleischer, J. Lin, J. K. Rosenstein, M. Drndić, and K. L. Shepard, Nano Lett. **16**, 4483 (2016).
[40]J. K. Rosenstein, M. Wanunu, C. A. Merchant, M. Drndic, and K. L. Shepard, Nat. Methods **9**, 487 (2012).
[41]C.-C. Chien, S. Shekar, D. J. Niedzwiecki, K. L. Shepard, and M. Drndić, ACS Nano **13**, 10545 (2019).
[42]M. Wanunu, J. Sutin, B. McNally, A. Chow, and A. Meller, Biophys. J. **95**, 4716 (2008).
[43]D. J. Niedzwiecki and L. Movileanu, J. Vis. Exp. **58**, e3560 (2011).
[44]D. J. Niedzwiecki, Y.-C. Chou, Z. Xia, F. Thei, and M. Drndić, Rev. Sci. Instrum. **91**, 031301 (2020).